JOURNAL OF PROPULSION AND POWER
Vol. 9, No. 5, Sept.–Oct. 1993

Injected Propellant Ionization in MPD Thrusters

Rodney L. Burton* and Nicholas Tiliakos†
University of Illinois at Urbana—Champaign, Urbana, Illinois 61801

A model is presented for the self-magnetized, weakly ionized preionization region at the entrance to a magnetoplasmadynamic (MPD) accelerator. The model is steady, one-dimensional and inviscid, and assumes supersonic flow of argon plasma with zero current in the region. Heavy particle temperature is constant, and electron temperature T_e is determined by ambipolar diffusion and by photo- and electron-impact ionization processes. The plasma continuity, momentum, and energy equations are integrated numerically with appropriate boundary conditions, giving a region width Δx ranging from 3 to 17 mm, depending on density, and a degree of ionization α increasing from an initial value of $\alpha = 10^{-7}$ to $\alpha = 4 \pm 2 \times 10^{-4}$ at the MPD accelerator inlet. The electron temperature rises monotonically from $T_e = 1000$ K to $T_e \cong 18{,}000$ K, a level sufficient to sustain MPD accelerator operation. The total electrostatic potential across Δx is $\Delta V = 12.5 \pm 0.6$ V. Reducing the injected particle flux Q_0 increases Δx, until a critical Q_0 is reached below which no solutions exist.

Nomenclature

$\mathbf{B}$ = magnetic field, T
E_x, E_y = laboratory electric field, V/m
E_ϕ = average excess energy of ionizing photoelectrons, eV
f' = photon fraction with $h\nu > E_I$
G = electron temperature gradient, dT_e/dx
h = Planck's constant, J-s
$\mathbf{j}$ = current density, A/m^2
L = arc length in flow direction, m
l_{Ross} = Rosseland mean free path, m
n = particle density, m^{-3}
n_n = neutral particle density, m^{-3}
n_0 = total heavy particle density, m^{-3}
p_e = electron pressure, Pa
Q_{ei} = coulomb cross section, m^2
Q_{en} = electron-neutral cross section, m^2
Q_0 = particle flux $n_0 u$, particles/m^2-s
$\boldsymbol{q}_e$ = electron heat flux vector, W/m^2
r_L = Larmor radius, m
T, T_e = heavy particle, electron temperature, K
T_{ex} = excitation temperature, K
u, v = axial, transverse mass average velocity, laboratory reference frame, m/s
V = electron/ion ambipolar diffusion velocity, m/s
V_n = neutral diffusion velocity, m/s
Δx = preionization width, $(x_1 - x_0)$, m
α = degree of ionization
Γ_{ex} = excitation rate, excitations/m^3-s
Γ_i = electron impact ionization rate, electrons/m^3-s
Γ_r = recombination rate, atoms/m^3-s
Γ_ϕ = photoionization rate, electrons/m^3-s
κ_e = electron thermal conductivity, W/m K
ν = collision frequency, s^{-1}
Ω_e = electron hall parameter

Constants
E_I = argon ionization potential, J
e = electron charge, C
k = Boltzman constant, J/K
M = ion mass, kg
m = electron mass, kg
S = slope of argon excitation cross section, m^2/J

Received Nov. 12, 1991; revision received Sept. 20, 1992; accepted for publication Dec. 11, 1992.

*Associate Professor, 306 Talbot Laboratory, 104 S. Wright St. Associate Fellow AIAA.
†Graduate Student. Student Member AIAA.

I. Introduction

THE magnetoplasmadynamic (MPD) thruster is one of a class of $\mathbf{j} \times \mathbf{B}$ accelerators being investigated for space propulsion applications.[1–5] The interelectrode region of this device has been well studied, both experimentally[6–16] and numerically,[17–23] generating an understanding into the complex physics of the acceleration process. However, little attention has been paid to the upstream region, where no current flows and into which the cold propellant gas is injected. Numerical models of the interelectrode region have therefore been forced to assume an ionization boundary condition at the entrance to the acceleration region, typically using $\alpha = 0.01$.[19,22,24] In this article we find that a lower value of α is more appropriate.

Previous efforts at studying the upstream region, which we call the preionization region, have adopted various physical models. Sheppard and Martinez-Sanchez[25] neglected radiation processes and assumed infinite electron thermal conductivity, giving constant electron temperature. The electrons were assumed to be energetically decoupled from the ions and neutrals, resulting in a nonequilibrium three-component plasma model. Burton and Tiliakos[26] also neglected radiation processes, but assumed a nonequilibrium three-component plasma model with finite electron thermal conductivity and electron impact ionization, resulting in a preionization region with electron temperature varying over a narrow range.

In this article the goal is to develop a consistent description of the preionization region of a MPD accelerator, from the point of cold gas injection to the entrance of the interelectrode current region, with plasma properties dependent only on the selection of appropriate boundary values. We adopt a physical model which includes radiation processes and the effect of the self-induced magnetic field on electron thermal conductivity.

The initial creation of electrons upstream of a MPD arc region by a photoionization mechanism is related to the creation of precursor regions or ionization fronts ahead of radiating shocks. Precursor regions and related ionization processes have been studied by a number of authors, as applied to the electromagnetic shock tube,[27] to shock fronts in air,[28–31] and to the ionizing region of a plasma focus device.[32] Radiation effects of ionizing shock waves in various gases have been discussed by several authors.[33–36]

II. Model Geometry

The analysis is applied to a self-field MPD accelerator, for which the flow is assumed steady and one-dimensional, with flow velocity in the positive x direction in Cartesian coordinates (Fig. 1). The preionization region, in which $\mathbf{j}$ is zero, is bounded by dielectric walls, the surface charge on which sustains E_x and E_y at the boundaries. Argon gas is injected at flow rate Q_0 through the porous dielectric injection wall at temperature T_0, located at x_0. The porous structure of the injection wall is assumed to be equivalent to a large number of converging-diverging micronozzles, from which the argon emerges at position x_0, flowing supersonically toward the inlet of the MPD accelerator located at x_1 (Fig. 1). The region width is $\Delta x = x_1 - x_0$. Electrode fringe fields at x_1 are neglected, and between the MPD electrodes the current density is j_y, with $j_x = 0$. The constant magnetic field $\mathbf{B}_z$ in the preionization region is in the $+z$ direction.

The argon in the preionization region is weakly ionized ($\alpha << 1$), with mass-averaged axial velocity u. The transverse velocity v is assumed zero, a condition which requires an E_y field. Energy coupling between the electrons at temperature $T_e(x)$ and the heavy particles at temperature T is weak, so that T is assumed constant in the preionization region. Viscosity is neglected, and electron-ion recombination is negligible. The flow does not accelerate in the region, because $\mathbf{j} \times \mathbf{B} = 0$, and for $\alpha << 1$, $u_n = u =$ constant.

III. Governing Equations

A simple ionization model is adopted in the preionization region by incorporating two possible processes: 1) electron-neutral impact ionization and 2) photoionization. Processes such as photoexcitation plus impact ionization, or impact excitation plus photoionization, are not included.

The electron impact ionization process is two-step, and the rate Γ_i is limited by the excitation rate of argon neutrals from the ground state.[34,37,38] Since Γ_i is negligible below $T_e = 10^4$ K and $\alpha \approx 10^{-5}$, photoionization is the only process by which α can be elevated from its initial low value at x_0. Bound-free photoionization has been previously identified as the appropriate process close to ionizing shock fronts,[31,36,39] equivalent to the near-arc region here. Although photoexcitation is occurring, for $\alpha < 10^{-5}$ there are too few electrons present to ionize the excited atom. We therefore assume that bound-free photoionization pertains, with the rate Γ_ϕ generated by arc photons with energy $h\nu$ greater than E_I. As α and T_e rise in the preionization region, a level is reached where Γ_i becomes dominant, leading to a value of α high enough at x_1 to sustain adequate current conduction in the interelectrode region.

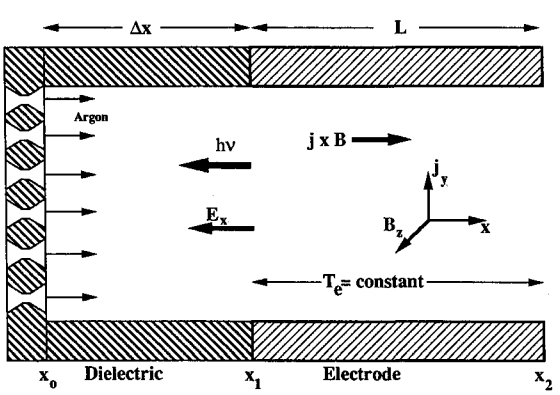

Fig. 1 Geometry of the interelectrode region of the MPD accelerator and the preionization zone. Cold argon propellant is injected through a series of micronozzles at x_0.

Electrons

For steady, one-dimensional conditions, with $n_e = \alpha n_0$, and n_0 constant in x for constant u, the electron continuity equation is

$$\frac{d(\alpha n_0 u_e)}{dx} = \Gamma_i + \Gamma_\phi \tag{1}$$

Solving for the gradient in electron species velocity

$$\frac{du_e}{dx} = \frac{\Gamma_i + \Gamma_\phi}{\alpha n_0} - \frac{u_e}{\alpha}\frac{d\alpha}{dx} \tag{2}$$

The electron momentum equation is expressed by Ohm's law. Since j_{ey} and v_e are zero, and since ion and neutral particle pressure gradients are neglected, the axial electric field is given by[40,41]

$$E_x = -\frac{1}{\alpha n_0 e}\frac{dp_e}{dx} \tag{3}$$

Rearranging Eq. (3) with $p_e = \alpha n_0 k T_e$ gives an expression for the gradient in α

$$\frac{d\alpha}{dx} = -\frac{\alpha e E_x}{kT_e} - \frac{\alpha G}{T_e} \tag{4}$$

The electron energy equation is written in the following form:

$$\alpha n_0 \left[u_e \frac{d(3kT_e/2)}{dx}\right] = -\frac{dq_e}{dx} + E_x j_e - \frac{3m}{M}\alpha n_0 k(T_e - T_i)\nu_c - V\frac{dp_e}{dx} - p_e\frac{du_e}{dx} - \Gamma_i(3kT_e/2 + E_I) - \Gamma_\phi(3kT_e/2 - E_\phi) \tag{5}$$

where $\nu_c = \nu_{ei} + \nu_{en}$.

The first term on the right side of Eq. (5) is the gradient in the heat flux, given by[41]

$$q_e = -\kappa_e\left(\frac{dT_e}{dx}\right) + 5\alpha n_0 k T_e V/2 \tag{6}$$

where κ_e is[41]

$$\kappa_e = \frac{5\alpha n_0 k^2 T_e}{3m\omega_B}\left(\frac{\Omega_e}{1 + \Omega_e^2}\right) \tag{7}$$

For a typical magnetic field of $B = 0.25$ T, Ω_e is $O[10^2]$, and the electrons gyrate around the B_z field lines. From Eq. (7), κ_e varies as $\alpha/(1 + \Omega e^2)$, and since $\alpha << 1$ and $\Omega_e >> 1$, κ_e is small in the preionization region. We therefore make the simplifying assumption $\kappa_e = 0$. Thus

$$q_e = 5\alpha n_0 k T_e V/2 \tag{8}$$

which represents electron heat transport driven by ambipolar diffusion.

The sixth term on the right side of Eq. (5) is the energy lost from the electron gas by impact ionization at rate Γ_i, including ionizing energy E_I and the cost of raising the new electrons to energy $3kT_e/2$. Similarly, the seventh term includes the energy cost for new electrons $3kT_e/2$ and the heating of the electron gas at rate $\Gamma_\phi E_\phi$ from photoionization at rate Γ_ϕ.

The conduction current is given by

$$j_e = -n_e e V \cong \alpha n_0 e(u_n - u_e) \tag{9}$$

where V is the ambipolar diffusion velocity.[41] The total collision-frequency $\nu_c = \nu_{ei} + \nu_{en}$ is evaluated with cross sections of $Q_{en} = 2 \times 10^{-20}$ m^2, and $Q_{ei} = 3.9 \times 10^{-10}\, \ell n\, \Lambda / T_e^2$ m^2,[42] where $\ell n\, \Lambda$ is taken as 10, and $T_e(x)$ is in Kelvin. Combining Eqs. (3) and (9) gives $j_e E_x = V(\mathrm{d}p_e/\mathrm{d}x)$, and cancels the second and fourth terms on the right side of Eq. (5).

The impact ionization rate is dominated by the rate of excitation Γ_{ex} of the first excited level of argon above the ground state, resulting in an ionization rate for $\alpha << 1$ of[37,38]

$$\Gamma_i = \Gamma_{ex} \cong [S(2k)^{3/2}/(\pi m)^{1/2}]\alpha n_0^2 T_e^{3/2}(T_{ex}/T_e + 2)e^{-T_{ex}/T_e} \tag{10}$$

where $S = 0.0044$ (m^2/J) is the slope of the argon excitation cross section for energies above threshold, and $T_{ex} = 133{,}500$ K.

An estimate of Γ_ϕ is required. Both the preionization and interelectrode regions are optically thin, with a Rosseland mean free path large compared to plasma axial length. The photoionization rate in the preionization region is then given by

$$\Gamma_\phi \cong \phi_i/(l_{Ross})_{pre} \tag{11}$$

The ionizing photon flux ϕ_i is approximated by assuming that the arc radiates as an optically thin gray body, with

$$\phi_i = \phi_{BB} f'(L/l_{Ross})_{arc} \tag{12}$$

The MPD arc discharge length L is typically 0.2 m, and $l_{Rossarc}$ is given by[43]

$$l_{Ross} = [(9.3 \times 10^{10})/n_n]T_{e1}^2 e(E_I/T_{e1}) \quad [\mathrm{m}] \tag{13}$$

where T_{e1} and E_I are here in Kelvin, n_n is in m^{-3}, and $\alpha << 1$. Typically, the arc is optically thin with $(L/l_{Ross})_{arc} = 0.02$.

The blackbody photon flux ϕ_{BB} is[44]

$$\phi_{BB} = \int_0^\infty \left[\frac{I_\nu(T_{e1})}{h\nu}\right] \mathrm{d}\nu = \int_0^\infty \frac{2\nu^2/c^2}{e^{(h\nu/kT_{e1})} - 1}\, \mathrm{d}\nu \tag{14}$$

The parameter f' is the fraction of photons with sufficient energy to ionize

$$f' = \frac{1}{\phi_{BB}} \int_{\nu_i}^\infty \frac{2\nu^2/c^2}{e^{h\nu/kT_{e1}} - 1}\, \mathrm{d}\nu \tag{15}$$

For an arc with temperature $T_{e1} = 18{,}500$ K, $f' = 0.0026$.

For typical conditions in the arc and preionization region, $\Gamma_\phi \approx 10^{22}$–$10^{25}$ electrons/m^3-s, constant throughout the preionization region since $(l_{Ross})_{pre} > \Delta x$. Each photoionization event heats the electron gas by energy $E_{\phi m} = h\nu - h\nu_i$,[39] except for a region near x_0. Within distance r_L of x_0 [$\sim 2 \times 10^{-5}$ m] the gyrating photoelectrons collide with the injection wall, transferring energy and reducing the electron energy to the wall temperature. Photoelectrons which do not strike the wall drift downstream at velocity u_{e0}. If t_{ee} is the equilibration time for energy transfer, these electrons drift a distance $u_{e0}t_{ee}$ before giving up their energy to the electron gas. E_ϕ is therefore taken as

$$\begin{aligned} E_{\phi 0} &= kT_0/e[\mathrm{eV}] \text{ for } x_0 < x < r_L \quad [\text{near wall}] \\ E_\phi &= E_{\phi m}[\mathrm{eV}] \text{ for } u_{e0}t_{ee} < x < x_1 \quad [\text{far from wall}] \end{aligned} \tag{16a}$$

where

$$E_{\phi m} = \frac{\int_{\nu_i}^\infty \frac{(h\nu)(2\nu^2/c^2)}{(e^{h\nu/kT_{e1}} - 1)}\, \mathrm{d}\nu}{\int_{\nu_i}^\infty \frac{(2\nu^2/c^2)}{(e^{h\nu/kT_{e1}} - 1)}\, \mathrm{d}\nu} - E_I \quad [\mathrm{eV}] \tag{16b}$$

and $\nu_i = E_I/h$. $E_{\phi m}(T_{e1})$ is approximated by $E_{\phi m}[\mathrm{eV}] \cong 1.4T_{e1}$, [eV] $- 0.3$, and is typically 1.9 eV. For x in the range $r_L < x < u_{e0}t_{ee}$, E_ϕ increases monotonically to $E_{\phi m}$, with a complex functional dependence derived from the tail of the Planck photon energy distribution, the coulomb cross section, and $\alpha(x)$. Because $u_{e0}t_{ee} \approx 10^{-3}$ m, small compared to the width of the region, E_ϕ is for simplicity assumed to increase linearly from $E_{\phi 0}$ to $E_{\phi m}$ for $r_L < x < u_{e0}t_{ee}$.

The energy equation with $\kappa_e = 0$ in Eq. (6) is now written as

$$\alpha n_0 \left[u_e \frac{\mathrm{d}(3kT_e/2)}{\mathrm{d}x}\right] = -\frac{\mathrm{d}}{\mathrm{d}x}(5p_e V/2) - \frac{3m}{M}(p_e - p_i)\nu_c - p_e \frac{\mathrm{d}V}{\mathrm{d}x} - \Gamma_i(3kT_e/2 + E_I) - \Gamma_\phi(3kT_e/2 - E_\phi) \tag{17}$$

Heavy Particles

For $u_i = u_e$, $\alpha << 1$, and u_n and T_i constant: $V_n = \alpha(u_n - u_i)$ and $V = V_i = V_e = -(u_n - u_i)$. Neglecting ion pressure and inertia terms, the ion momentum equation in the preionization region is[24,26,41]

$$\alpha n_0 M \nu_{in}(u_n - u_i)/2 + M(\Gamma_i + \Gamma_\phi)(u_n - u_i) + \alpha n_0 e E_x = 0 \tag{18}$$

The ion-neutral collision frequency ν_{in} includes elastic and charge exchange collisions, giving a momentum production rate balanced by ionization and the axial electric field. The ion-neutral collision cross section, Q_{in} is taken as 1.4×10^{-18} m^2.[45,46]

Equation (18) gives for the axial electric field

$$eE_x = -M(u_n - u_i)\nu_{eff} = MV\nu_{eff} \tag{19}$$

where

$$\nu_{eff} = [\nu_{in}/2 + (\Gamma_i + \Gamma_\phi)/\alpha n_0] \tag{20}$$

From Eqs. (3) and (19) it is seen that eE_x is generated by $\mathrm{d}p_e/\mathrm{d}x$, and opposed by the momentum transfer of ions diffusing through neutrals with an effective collision frequency ν_{eff}, the result of elastic and charge exchange collisions, and the net ionization rate $(\Gamma_i + \Gamma_\phi)$.

The assumption that the flow is one-dimensional with $\mathbf{j} = 0$, $\mathrm{d}p_{e,i}/\mathrm{d}y = 0$ and $v_e = v_i = v = 0$ requires the existence of an E_y field, where $E_y(x)$ is established by a charge layer on the dielectric walls. Using Ohm's law for a partially ionized plasma,[41] modified for $\alpha << 1$ and $T_n << T_e$, and combining with Eqs. (3), (19), and (20) gives

$$E_y = [u_n - (u_n - u_i)(\nu_{eff}/\nu_{in})]B_z$$

The transverse field E_y is therefore equal to $u_n B_z$, corrected by ion diffusion and ionization rate.

Boundary Conditions

The temperatures and temperature gradients are specified at x_0 and x_1. At x_0 (Fig. 1) the gyrating electrons within one Larmor radius of the wall are assumed to equilibrate at the injection temperature, giving $T_e(x_0) = T_0$. Furthermore, $T_e = T_0$ is assumed for the range $x_0 < x < r_L$, giving the condition $G \equiv \mathrm{d}T_e/\mathrm{d}x = 0$ at x_0. This condition assures zero conductive

heat flux by the electrons into the wall, despite $\kappa_e \neq 0$ for $x_0 < x < r_L$.

The preionization solution is patched at x_1 to a previously-determined one-dimensional solution for the arc region, in which T_e is assumed constant, and for which T_e is typically 18,600 K.[24,26,47] With $G = 0$ in the arc, the same condition is assumed at x_1 for the preionization solution, and is used in the numerical integration as a condition establishing the x_1 location. The value $T_e(x_1) = T_{e1}$ is not specified, but must be in the range of 18,000 ± 1000 K to allow arc solutions with reasonable lengths $L < 1$ m.

Arc solutions were previously found to exist for a narrow range of the parameter $B_z^2/m_i n_0 u_n$,[24,26] equivalent to the coaxial MPD thruster parameter $J^2/(\mathrm{d}m/\mathrm{d}t)$, where J is thruster current and $\mathrm{d}m/\mathrm{d}t$ is propellant flow rate.[1] All calculations are performed here for a single value of $B_z^2/m_i n_0 u_n = 0.022$, mks, equivalent to a $J^2/(\mathrm{d}m/\mathrm{d}t)$ value of ~20 [kA²/(g/s)], a stable operating regime below the critical "onset" mode.[1,23]

Flow through the injection wall is assumed isentropic, with total temperature $T_0 = 1000$ K, and the flow Mach number treated as a variable, with $1 < M < 3$. The neutral particle velocity is assumed constant for $x_0 < x < x_1$ and is given by $u_n = a_0 M/(1 + M^2/3)^{1/2}$ with $a_0 = (\gamma R T_0)^{1/2}$ and $\gamma = \frac{5}{3}$.

It is assumed that a low background level of ionization α_0 exists at x_0, created by photoionization. The lowest α_0 which can be used with the continuum assumption for the electron gas is $\alpha_0 \approx 10^{-7}$, at which level the mean free path is several millimeters, as determined by coulomb collisions. Conditions at x_1 are found to be insensitive to the choice of α_0 for $\alpha_0 < 10^{-6}$. The ionization level at all $x \leq x_1$ is not specified but is determined by the model, as are E_x, T_e, and u_e.

Since $G(x_0) = 0$, $E_x(x_0)$ is analytically determined. Combining Eqs. (2), (4), (17), and (19) with $\alpha^2 \ll 1$ and $\Gamma_i \approx 0$ gives a quadratic equation for $E_x(x_0)$, where $E_x(x_0)$ is a function of α_0, T_0 and Γ_ϕ. $E_x(x_0)$ is typically found to be -200 V/m for $\Gamma_\phi = 10^{22}$ electrons/m³-s.

IV. Numerical Method

Equations (2), (4), and (17) represent a system of highly coupled first-order nonlinear ordinary differential equations. The equations are solved using a fourth-order Runge-Kutta routine with adaptive step size control. The procedure solves for the first derivatives of u_e, α, and T_e from Eqs. (2), (4), and (17). The integration begins at $x_0 = 0$, and steps to x_1 where $G(x_1) = 0$, the inlet to the MPD accelerator.

Solutions are sought for which the electron temperature and ionization fraction increase monotonically from x_0 to x_1, yielding profiles of T_e, α, E_x, and u_e. Monotonically increasing T_e and α requires $\mathrm{d}u_e/\mathrm{d}x < 0$ from Eq. (2), and $E_x < 0$ from Eq. (19), resulting in higher ambipolar diffusion velocity and gradient $\mathrm{d}p_e/\mathrm{d}x$ near x_1.

V. Results

Solutions are shown in Figs. 2–7 for baseline conditions of $T_0 = 1000$ K, $\alpha_0 = 10^{-7}$, neutral particle flux of $(Q_0)_b = 4.27 \times 10^{25}$ particles/m²-s, $B_z = 0.25$ T, and $\Gamma_\phi = 10^{22}$ photoelectrons/m³-s, for neutral particle Mach numbers for $1 < M < 3$. These baseline conditions are known to produce valid solutions of the arc model.[24,26] The resulting T_{e1} and α_1 at $x = x_1$ are shown in Figs. 2 and 3. T_{e1} lies in the range of 17,600–18,850 K and α_1 falls in the relatively narrow range of $3.4–5.6 \times 10^{-4}$ for $1 < M < 3$. The width Δx of the preionization region increases with Mach number, from $\Delta x = 3.2$ mm at $M = 1$ to $\Delta x = 5.9$ mm at $M = 3$.

Profiles of E_x and u_e are shown for baseline conditions in Figs. 4 and 5. E_x rises rapidly near x_0 from -230 V/m to ~ -1500 V/m, plateaus, and then increases to a second plateau at x_1. E_{x1} varies from -5800 V/m at $M = 1$ to -3400 V/m at $M = 3$. The electron species velocity u_e at the inlet is observed to follow the same plateau behavior as E_x as the Mach number increases from $M = 1$ to 3. At all Mach numbers u_e is less than u_n at x_0, and decreases to minimum at x_1 of ~130 m/s.

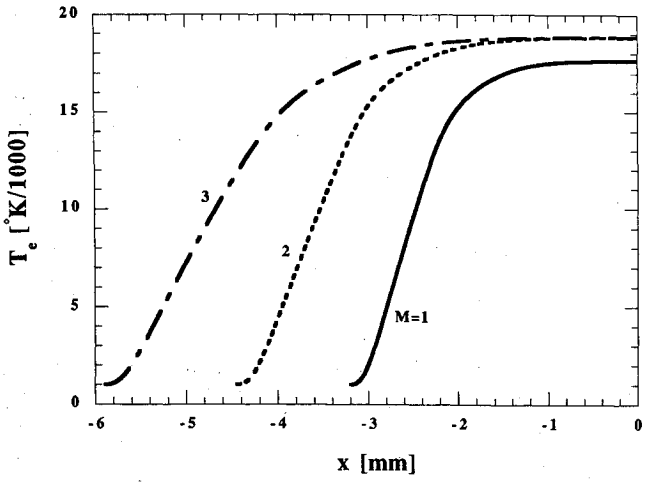

Fig. 2 Electron temperature profiles for $M = 1, 2, 3$ with x_1 at $x = 0$. $(Q_0)_b = 4.27 \times 10^{25}$ (m²-s)$^{-1}$, $T_0 = 1000$ K, $\alpha_0 = 10^{-7}$ and $\Gamma_\phi = 10^{22}$ photoelectrons/m³-s.

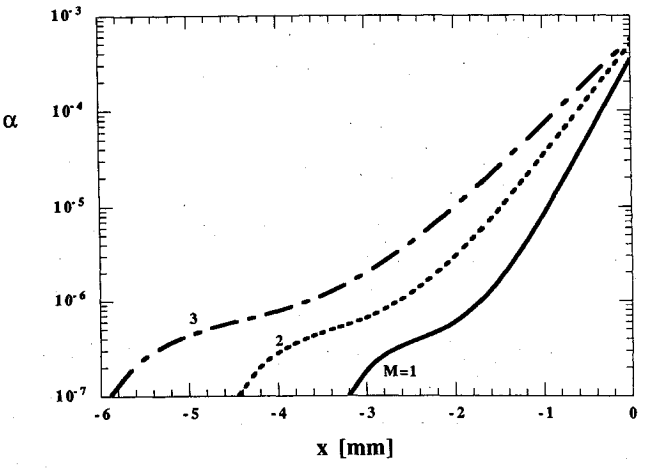

Fig. 3 Ionization fraction profiles for conditions of Fig. 2.

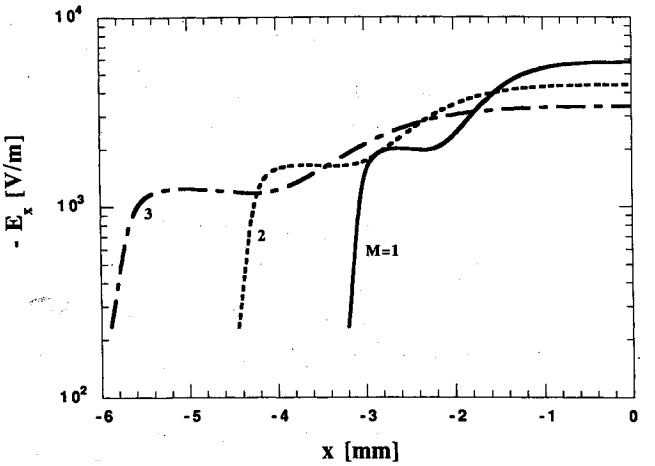

Fig. 4 Axial electric field profiles for conditions of Fig. 2.

An electric potential across the region can be calculated, given by

$$\Delta V = -\int_{x_0}^{x_1} E_x \, \mathrm{d}x$$

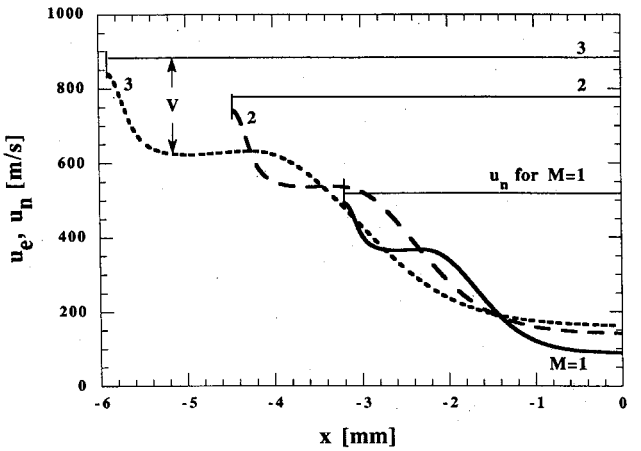

Fig. 5 Charged particle velocity profiles for conditions of Fig. 2. The neutral velocity is constant, and ambipolar diffusion velocity $V = (u_e - u_n)$.

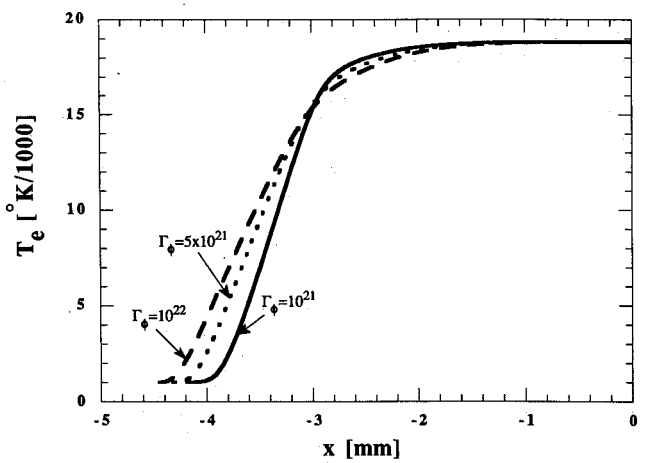

Fig. 6 Effect of Γ_ϕ on electron temperature profiles for $M = 2$, $(Q_0)_b = 4.27 \times 10^{25}$ (m^2-s)$^{-1}$, $T_0 = 1000$ K, and $\alpha_0 = 10^{-7}$.

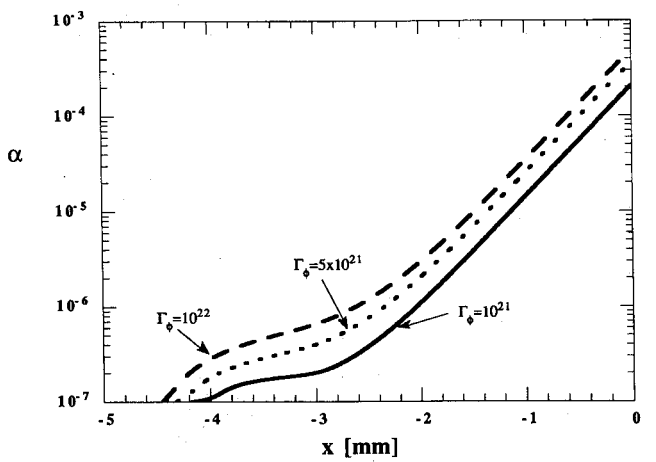

Fig. 7 Effect of Γ_ϕ on α for conditions of Fig. 6.

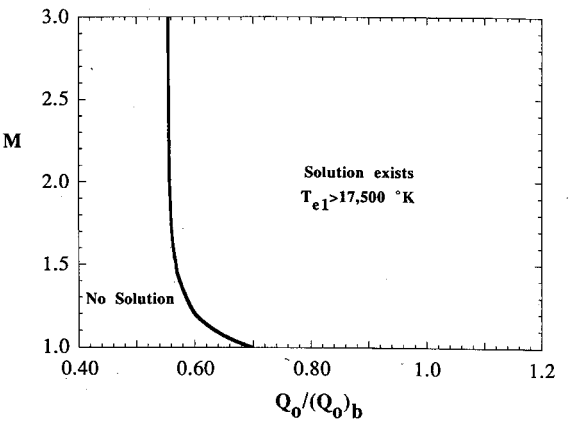

Fig. 8 Solution regime. No solution exists for $Q_0/(Q_0)_b < 0.55$.

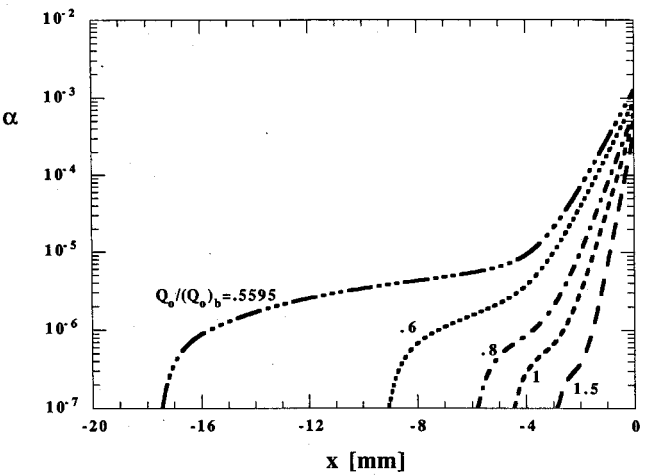

Fig. 9 Ionization fraction profiles vs $Q_0/(Q_0)_b$ at $M = 2$.

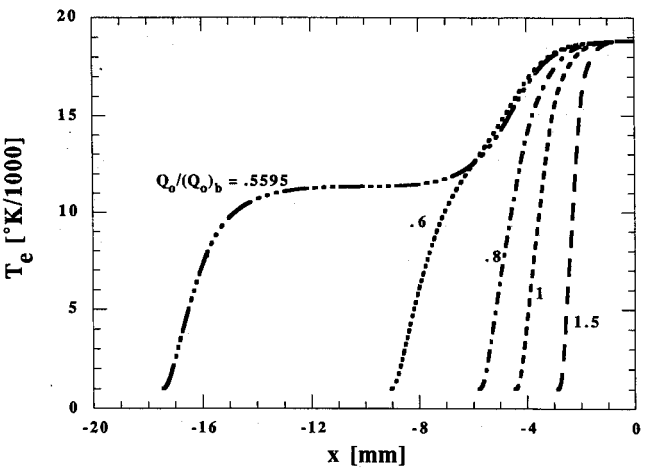

Fig. 10 Electron temperature profiles vs $Q_0/(Q_0)_b$ at $M = 2$.

which is found to be relatively constant. For $M = 1$, $\Delta x = 3.2$ mm and $\Delta V = 11.84$ V. For $M = 3$, $\Delta x = 5.9$ mm and $\Delta V = 12.86$ V. Note that ΔV is on the order of the ionization potential E_I.

The sensitivity of T_{e1} and α_1 to the photoionization rate Γ_ϕ, for Mach 2.0 and $(Q_0)_b = 4.27 \times 10^{25}$ particles/m^2-s, is displayed in Figs. 6 and 7. Reducing Γ_ϕ by an order of magnitude to 10^{21} has a small effect on $\alpha(x)$ and $T_e(x)$, narrowing the preionization region by <1 mm, and reducing α_1 from 4.9×10^{-4} ($\Gamma_\phi = 10^{22}$) to 2.1×10^{-4} ($\Gamma_\phi = 10^{21}$). The effect on T_e is appreciable far upstream, but is negligible near x_1, where the difference is only a few Kelvin.

Not all values of particle flux Q_0 lead to solutions which match arc conditions. For Q_0 sufficiently below the baseline value $(Q_0)_b$, no solution is found that simultaneously satisfies T_{e1} and $E_{\phi m}(T_{e1})$. The solution boundary, which depends on Mach number for $0.55 < Q_0/(Q_0)_b < 0.70$, is shown in Fig. 8. For Q_0 and M values to the right of the boundary, solutions exist with $T_{e1} > 17{,}500$ K. No solutions are found at any Mach

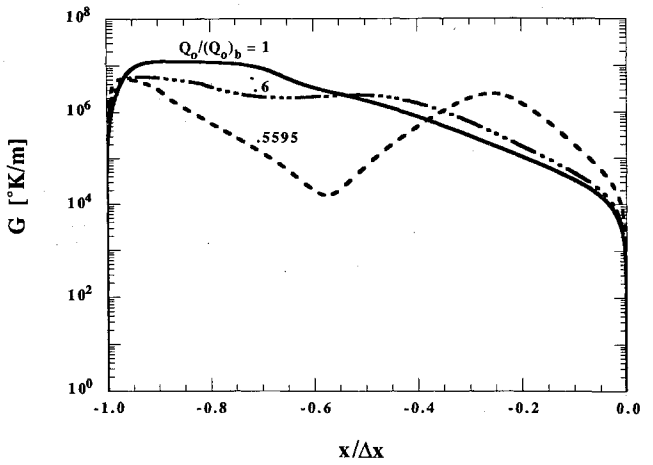

Fig. 11 Profiles of electron temperature gradient G for flow rates approaching the critical value.

number for $Q_0/(Q_0)_b < 0.55$, thereby establishing a critical value of Q_0.

As shown in Figs. 9 and 10, reducing Q_0 has the effect of increasing the width of the preionization region. As $Q_0/(Q_0)_b$ is varied from 1.50 to 0.5595 (with $M = 2$ and $\Gamma_\phi = 10^{22}$), and B_z^2 is also varied to keep $B_z^2/m_i Q_0$ constant, Δx increases from 2.9 to 17.5 mm. This variation in Q_0 changes T_{e1} by only a few Kelvin, and has a relatively small effect on α_1. The electric potential across Δx varies from $\Delta V = 13.1$ to 12.2 V over this range.

VI. Discussion and Conclusions

The results show that while photoionization is essential for initiating the ionizing process, the $\alpha(x)$ and $T_e(x)$ profiles are not sensitive to an order-of-magnitude change in Γ_ϕ, suggesting that ionization cannot be solely supported by radiation throughout the region. Proceeding downstream, α rises by photoionization to a level of $\sim 10^{-5}$, accompanied by a rise in electron temperature to ~15,000 K, where Γ_i becomes dominant. This process is then followed by a further increase in α to $\sim 4 \times 10^{-4}$ at x_1.

Reducing the particle density n_0 in the region, either by increasing M at constant Q_0, or by decreasing Q_0 at constant M, has the effect of increasing Δx. This behavior is presumably connected to the impact ionization process since $\Gamma_i > \Gamma_\phi$ over most of the preionization region, and from Eq. (10), Γ_i varies as n_0^2. Since $\Delta V = -\int E_x \, dx$ is approximately invariant, increasing Δx reduces the average $\langle E_x \rangle = \Delta V/\Delta x$ in the region. This rapidly reduces dp_e/dx, which varies as $n_0 E_x$ from Eq. (3).

With $\kappa_e = 0$, electron heating occurs primarily from ambipolar diffusion, and to a lesser extent from radiation. Rapidly reducing dp_e/dx reduces the electron heat flux q_e [Eq. (8)]. As shown in Figs. 10 and 11, at the critical value of particle flux $Q_0/(Q_0)_b = 0.5595$, the gradient $G = dT_e/dx$ decreases by several orders of magnitude in the center of the region. A slight further reduction in Q_0 drives G towards zero, halting the ionization process and preventing solutions which satisfy accelerator inlet conditions.

Acknowledgments

Support for this work by TRW Space and Technology Group, under the University of Illinois Industrial Affiliates Program in Electric Propulsion, and by the Department of Aeronautical and Astronautical Engineering, is gratefully acknowledged.

References

[1]Sovey, J. S., and Mantenieks, M. A., "Performance and Lifetime Assessment of Magnetoplasmadynamic Arc Thruster Technology," *Journal of Propulsion and Power*, Vol. 7, No. 1, 1991, pp. 71–83.

[2]Gilland, J. H., and Myers, R. M., "Multimegawatt Electric Propulsion System Design Considerations," AIAA/DGLR/JSASS 21st International Electric Propulsion Conf., IEPC 90-2552, Orlando, FL, July 1990.

[3]Wegmann, T., Auweter-Kurtz, M., Kurtz, H. L., Merke, W., Loesener, O., and Schrade, H. O., "Steady State High Power MPD Thrusters," AIAA/DGLR/JSASS 21st International Electric Propulsion Conf., IEPC 90-2555, Orlando, FL, July 1990.

[4]Tahara, H., Kagaya, Y., and Yoshikawa, T., "Quasisteady Magnetoplasmadynamic Thruster with Applied Magnetic Fields for Near-Earth Missions," *Journal of Propulsion and Power*, Vol. 5, No. 6, 1989, pp. 713–717.

[5]King, D. Q., "Feasibility of Steady-State, Multi-Megawatt MPD Thrusters," AIAA/DGLR/JSASS 18th International Electric Propulsion Conf., IEPC 85-2004, Alexandria, VA, Sept.–Oct. 1985.

[6]Hugel, H., Kruelle, G., and Peters, T., "Investigations on Plasma Thrusters with Thermal and Self-Magnetic Acceleration," *AIAA Journal*, Vol. 5, No. 3, 1967, pp. 551–558.

[7]Burton, R. L., Clark, K. E., and Jahn, R. G., "Measured Performance of a Multimegawatt MPD Thruster," *Journal of Spacecraft and Rockets*, Vol. 20, No. 3, 1983, pp. 299–304.

[8]Uematsu, K., and Morimoto, S., "MPD Thruster Performance with Various Propellants," *Journal of Spacecraft and Rockets*, Vol. 22, No. 4, 1985, pp. 412–416.

[9]Merfeld, D. J., Kelly, A. J., and Jahn, R. G., "MPD Thruster Performance: Propellant Distribution and Species Effects," AIAA/DGLR/JSASS 18th International Electric Propulsion Conf., IEPC 85-2022, Alexandria, VA, Sept.–Oct. 1985.

[10]Kurtz, H. L., Auweter-Kurtz, M., Merke, W. D., and Schrade, H. O., "Experimental MPD Thruster Investigations," AIAA/JSASS/DGLR 19th International Electric Propulsion Conf., IEPC 87-1019, Colorado Springs, CO, May 1987.

[11]King, D. Q., and Brophy, J. R., "Design and Operation of a 100 kW, Subscale MPD Engine," AIAA/DGLR/JSASS 19th International Electric Propulsion Conference, IEPC 87-1020, Colorado Springs, CO, May 1987.

[12]Mantenieks, M., Sovey, J. S., Myers, R. M., Haag, T. W., Raitano, P., and Parkes, J. E., "Performance of a 100 kW Class Applied Field MPD Thruster," AIAA/ASME/SAE/ASEE 25th Joint Propulsion Conf., AIAA Paper 89-2710, Monterey, CA, July 1989.

[13]Tahara, H., Sasaki, M., Kagaya, Y., and Yoshikawa, T., "Thruster Performance and Acceleration Mechanisms of a Quasi-steady Applied-field MPD Arcjet," AIAA/DGLR/JSASS 21st International Electric Propulsion Conf., IEPC 90-2554, Orlando, FL, July 1990.

[14]Heimerdinger, D. J., and Martinez-Sanchez, M., "Design and Performance of an Annular Magnetoplasmadynamic Thruster," *Journal of Propulsion and Power*, Vol. 7, No. 6, 1991, pp. 975–980.

[15]Sasoh, A., and Arakawa, Y., "Electromagnetic Effects in an Applied-Field Magnetoplasmadynamic Thruster," *Journal of Propulsion and Power*, Vol. 8, No. 1, 1992, pp. 98–102.

[16]Andrenucci, M., Paganucci, F., Frazzetta, M., La Motta, G., and Schianchi, G., "Scale Effects on the Performance of MPD Thrusters," AIDAA/AIAA/DGLR/JSASS 22nd International Electric Propulsion Conf., IEPC 91-123, Viareggio, Italy, Oct. 1991.

[17]Auweter-Kurtz, M., Kurtz, H. L., Schrade, H. O., and Sleziona, P. C., "Numerical Modeling of the Flow Discharge in MPD Thrusters," *Journal of Propulsion and Power*, Vol. 5, No. 1, 1989, pp. 49–55.

[18]Brushlinskii, K. V., Zaborov, A. M., Kozlov, A. N., Morozov, A. I., and Savel'ev, VV., "Numerical Modeling of Plasma Flow in High-Current Quasistationary Plasma Accelerators," *Soviet Journal of Plasma Physics*, Vol. 16, No. 2, 1990, pp. 79–85.

[19]Niewood, E., and Martinez-Sanchez, M., "Quasi One Dimensional Numerical Simulation of Magnetoplasmadynamic Thrusters," AIAA/DGLR/JSASS 21st International Electric Propulsion Conf., AIAA 90-2604, Orlando, FL, July 1990.

[20]Sleziona, P. C., Auweter-Kurtz, M., and Schrade, H. O., "Numerical Evaluation of MPD Thrusters," AIAA/DGLR/JSASS 21st International Electric Propulsion Conf., AIAA Paper 90-2602, Orlando, FL, July 1990.

[21]Martinez-Sanchez, M., "Structure of Self-Field Accelerated Plasma Flows," *Journal of Propulsion and Power*, Vol. 7, No. 1, 1991, pp. 56–64.

[22]Niewood, E. H., and Martinez-Sanchez, M., "A Two-Dimensional Model of an MPD Thruster," AIAA/SAE/ASME/ASEE 27th Joint Propulsion Conf., AIAA Paper 91-2344, Sacramento, CA, July 1991.

[23]LaPointe, M. R., "Numerical Simulation of Self-Field MPD Thrusters," AIAA/SAE/ASME/ASEE 27th Joint Propulsion Conf., AIAA Paper 91-2341, Sacramento, CA, July 1991.

[24]Devillers, J. P., "The Acceleration Processes in Magnetoplasma-Dynamic Arcs," Ph.D. Dissertation, Dept. of Aerospace and Mechanical Engineering Science, Univ. of California at San Diego, San Diego, CA, 1971.

[25]Sheppard, E. J., and Martinez-Sanchez, M., "Ionizational Ignition at the Inlet of an MPD Thruster," AIDAA/AIAA/DGLR/JSASS 22nd International Electric Propulsion Conf., IEPC 91-088, Viareggio, Italy, Oct. 1991.

[26]Burton, R. L., and Tiliakos, N., "Pre-Ionization Processes in a Self-Field MPD Accelerator," AIDAA/AIAA/DGLR/JSASS 22nd International Electric Propulsion Conf., IEPC 91-089, Viareggio, Italy, Oct. 1991.

[27]Barach, J. P., and Sivinski, J. A., "Measurements of a Precursor Electron Front," *Physics of Fluids*, Vol. 8, No. 12, 1965, pp. 2158–2161.

[28]Wetzel, L., "Precursor Effects and Electron Diffusion from a Shock Front," *Physics of Fluids*, Vol. 5, No. 7, 1962, pp. 824–830.

[29]Wetzel, L., "A Feature of Precursor Ionization Profiles due to Shock Radiation," *Physics of Fluids*, Vol. 5, No. 5, 1963, pp. 750–752.

[30]Biberman, L. M., and Veklenko, B. A., "Radiative Processes Ahead of a Shock-Wave Front," *Soviet Physics JETP*, Vol. 37(10), No. 1, 1960, pp. 117–120.

[31]Nelson, R. A., "Theories of Fast Luminous Fronts," *Physics of Fluids*, Vol. 8, No. 1, 1965, pp. 23–25.

[32]Bilbao, L., Kelly, H., and Bruzzone, H., "Radiation Transport in an Ionizing Current Sheath," *Physics of Fluids*, Vol. 29, No. 12, 1986, pp. 4182–4187.

[33]Weymann, H. D., "Electron Diffusion Ahead of Shock Waves in Argon," *Physics of Fluids*, Vol. 8, No. 1, 1965, pp. 23–25.

[34]Biberman, L. M., and Yakubov, I. T., "Approach to Ionization Equilibrium Behind the Front of a Shock Wave in an Atomic Gas," *Soviet Physics-Technical Physics*, Vol. 8, No. 11, 1964, pp. 1001–1007.

[35]Kuznetsov, N. M., "The Influence of Radiation on the Ionization Structure of the Front of a Shock Wave," *Soviet Physics-Technical Physics*, Vol. 9, No. 4, 1964, pp. 483–487.

[36]Liberman, M. A., and Velikovich, A. L., *Physics of Shock Waves in Gases and Plasma*, Springer-Verlag, New York, 1986, Chap. 2.

[37]Morgan, E. J., and Morrison, R. D., "Ionization Rates Behind Shock Waves in Argon," *Physics of Fluids*, Vol. 8, No. 9, 1965, pp. 1608–1615.

[38]Perona, G. E., and Axford, W. I., "Structure of a Normal Ionizing Shock Wave in Argon," *Physics of Fluids*, Vol. 11, No. 2, 1968, pp. 294–302.

[39]Clarke, J. H., and Ferrari, C., "Gas Dynamics with Nonequilibrium Radiative and Collisional Ionization," *Physics of Fluids*, Vol. 8, No. 12, 1965, pp. 2121–2139.

[40]Demetriades, S. T., and Argyropoulos, G. S., "Ohm's Law in Multicomponent Nonisothermal Plasma with Temperature and Pressure Gradients," *Physics of Fluids*, Vol. 9, No. 11, 1966, pp. 2136–2149.

[41]Sutton, G. W., and Sherman, A., *Engineering Magnetohydrodynamics*, McGraw-Hill, New York, 1965.

[42]Jahn, R. G., *Physics of Electric Propulsion*, McGraw-Hill, New York, 1968.

[43]Zel'dovich, Ya. B., and Raizer, Yu. P., *Physics of Shock Waves and High Temperature Hydrodynamic Phenomena*, Vols. I and II, Academic Press, New York, 1966.

[44]Vincenti, W. G., and Kruger, C. H., Jr., *Introduction to Physical Gas Dynamics*, Wiley, New York, 1967.

[45]Jaffrin, M. Y., "Shock Structure in a Partially Ionized Gas," *Physics of Fluids*, Vol. 8, No. 4, 1965, pp. 606–625.

[46]Mahadevan, P., and Magnuson, G. D., "Low-Energy (1- to 100-eV) Charge-Transfer Cross-Section Measurements for Noble-Gas-Ion Collisions with Gases," *Physical Review*, Vol. 171, No. 1, 1968, pp. 103–109.

[47]Randolph, T. M., von Jaskowsky, W. F., Kelly, A. J., and Jahn, R. G., "Ionization Processes in the Interelectrode Region of an MPD Thruster," AIDAA/AIAA/DGLR/JSASS 22nd International Electric Propulsion Conf., IEPC 91-052, Viareggio, Italy, Oct. 1991.